HHS Public Access

Author manuscript

*Cell Stem Cell*. Author manuscript; available in PMC 2015 November 19.

Published in final edited form as:

*Cell Stem Cell*. 2014 June 5; 14(6): 781–795. doi:10.1016/j.stem.2014.03.004.

# Pathways Disrupted in Human ALS Motor Neurons Identified Through Genetic Correction of Mutant *SOD1*

**Evangelos Kiskinis**[1,2,3,*], **Jackson Sandoe**[1,2,3,*], **Luis A. Williams**[1,2,3], **Gabriella L. Boulting**[1,2], **Rob Moccia**[1,2,3], **Brian J. Wainger**[4,5], **Steve Han**[1,2,3], **Theodore Peng**[1,2,3], **Sebastian Thams**[6], **Shravani Mikkilineni**[1,2,3], **Cassidy Mellin**[4], **Florian T. Merkle**[1,2,3], **Brandi N. Davis-Dusenbery**[1,2,3], **Michael Ziller**[2], **Derek Oakley**[6], **Justin Ichida**[1,2,3], **Stefania Dicostanza**[1,2], **Nick Atwater**[1,2,3], **Morgan L. Maeder**[7], **Mathew J. Goodwin**[7], **James Nemesh**[3,8,9], **Robert E. Handsaker**[3,8,9], **Daniel Paull**[10], **Scott Noggle**[10], **Steven A. McCarroll**[3,8,9], **J. Keith Joung**[7], **Clifford J. Woolf**[4], **Robert H Brown**[8], and **Kevin Eggan**[1,2,3,†]

[1]The Howard Hughes Medical Institute, USA

[2]Harvard Stem Cell Institute, Department of Stem Cell and Regenerative Biology, Harvard University, Cambridge, MA, 02138, USA

[3]Stanley Center for Psychiatric Research, Broad Institute of Harvard and MIT, Cambridge, MA, 02138, USA

[4]FM Kirby Neurobiology Center, Boston Children's Hospital and Department of Neurobiology, Harvard Medical School, Boston, MA, 02115, USA

[5]Department of Anesthesia, Critical Care and Pain Medicine, Massachusetts General Hospital, Boston, MA, 02115, USA

[6]Project A.L.S./Jenifer Estess Laboratory for Stem Cell Research, Depts. Pathology, Neurology and Neuroscience, Columbia University, Center for Motor Neuron Biology and Disease (MNC), and Columbia Stem Cell Initiative (CSCI), New York, NY, 10027, USA

[7]Molecular Pathology Unit, Center for Computational and Integrative Biology, and Center for Cancer Research, Massachusetts General Hospital, Charlestown, MA 02129 USA

[8]Department of Neurology, University of Massachusetts Medical School, Worcester MA 01655, USA

[9]Department of Genetics, Harvard Medical School, Boston, MA, 02115, USA

[10]The New York Stem Cell Foundation Research Institute, New York, NY, 10023, USA

## Summary

[†]Corresponding Author: Kevin Eggan, Phone: 617 496-5611, Fax: 617 384-8234, eggan@mcb.harvard.edu.
[*]These authors contributed equally

Supplemental Information: Supplemental Information for this article includes 7 figures and 3 tables.

Although many distinct mutations in a variety of genes are known to cause Amyotrophic Lateral Sclerosis (ALS), it remains poorly understood how they selectively impact motor neuron biology and whether they converge on common pathways to cause neuronal degeneration. Here, we have combined reprogramming and stem cell differentiation approaches with genome engineering and RNA sequencing to define the transcriptional and functional changes that are induced in human motor neurons by mutant *SOD1*. Mutant SOD1 protein induced a transcriptional signature indicative of increased oxidative stress, reduced mitochondrial function, altered sub-cellular transport as well as activation of the ER stress and unfolded protein response pathways. Functional studies demonstrated that these pathways were perturbed in a manner dependent on the *SOD1* mutation. Finally, interrogation of stem cell-derived motor neurons produced from ALS patients harboring a repeat expansion in *C9orf72* indicates at least a subset of these changes are more broadly conserved in ALS.

## Introduction

ALS is a fatal neurological condition characterized by death of motor neurons (MNs) (Hardiman et al., 2011). Classical linkage studies and DNA sequencing approaches have demonstrated that ALS can be caused by a variety of mutations in more than two dozen genes acting on diverse cellular functions (Sreedharan and Brown, 2013). Mutations in *SUPEROXIDE DISMUTASE 1* (*SOD1*) were originally identified through their autosomal dominant inheritance pattern (Rosen et al., 1993). More recently, genome wide association studies, DNA sequencing efforts and linkage analysis have all contributed to the identification of a hexanucleotide repeat expansion at *C9orf72* as a cause of ALS in an ample fraction of both familial and sporadic cases (DeJesus-Hernandez et al., 2011; Renton et al., 2011; Robberecht and Philips, 2013).

The discovery of *SOD1* mutations led to widely studied transgenic rodent models of ALS (Gurney et al., 1994; Howland et al., 2002). While indisputably valuable, these animals as well as many cell-based models (Oh et al., 2008; Wada et al., 2012), overexpress heterologous human SOD1 at super-physiological levels. Therefore, it is generally accepted that findings from these systems carry the caveat that they could be artifacts of protein overexpression (Gladman et al., 2012). Moreover, there is little information on how SOD1 impacts human MNs, leaving open to what extent results from the *SOD1* rodent models are relevant to understanding ALS in the human nervous system.

In addition, identification of patient mutations in other genes, such as *TDP43* (Sreedharan et al., 2008) and *C9orf72* (DeJesus-Hernandez et al., 2011; Renton et al., 2011) have not yet translated into the creation of animal models that are as widely accepted as *SOD1* transgenic mice (Sreedharan and Brown, 2013). As a result, understanding whether mutant *SOD1*-induced changes in MNs are relevant to other genetic types of ALS, has been slow to develop. Identification of shared mechanisms of MN disease could inform the selection of pathways for therapeutic intervention with the greatest relevance to a broader patient population.

We and others have proposed that induced pluripotent stem cells (iPSCs) from ALS patients and their differentiation into spinal MNs (Dimos et al., 2008) could complement existing

animal models, allowing hypotheses to be tested in human MNs with the patients' unique genetic constellation (Bilican et al., 2012; Donnelly et al., 2013; Egawa et al., 2012; Sareen et al., 2013).

Here, we have combined reprogramming and stem cell differentiation approaches with genome engineering and RNA sequencing technologies to identify the transcriptional and functional changes induced by the *SOD1A4V* mutation in human MNs. In addition to supporting hypotheses concerning the actions of mutant SOD1 protein developed using transgenic mouse models, such as the disruption of mitochondrial function and transport, our studies identified novel mechanisms that may contribute to MN dysfunction. Notably, we found that mutant SOD1 disrupts a delicate balance between ER stress and neuronal excitability that is inherent to MNs. Finally, studies using iPSCs derived from patients harboring *C9orf72* repeat expansions indicate that at least a subset of the changes induced by mutant *SOD1* in human MNs are relevant to both forms of ALS.

## Results

### Generation of iPSCs and Functional Motor Neurons from *SOD1$^{+/A4V}$* ALS Patients

We derived skin fibroblasts from two female ALS patients (study participants 39 and RB9) carrying the same dominantly acting *SOD1*A4V mutation (*SOD1$^{+/A4V}$*). We then generated iPSCs via retroviral transduction of *OCT4*, *SOX2* and *KLF4* and validated their integrity through a battery of standard pluripotency assays (Table S1). We then obtained differentiated spinal MNs through modest modifications to a previously reported protocol (Figure 1A, Figure S1A) (Boulting et al., 2011), which resulted in highly neuralized cultures (TUJ1+>97%), with significant percentage of ISL+ and HB9+ postmitotic MNs (Figures S1-2). Our MN cultures were electrophysiologically active (Figure S1D-G) and could functionally integrate into the developing chick spinal cord (Figure S2D-E).

### Increased Apoptosis and Altered Morphometry in *SOD1$^{+/A4V}$* Motor Neurons

To ask whether *SOD1$^{+/A4V}$* MNs manifest a phenotype under standard culture conditions we compared them with MNs produced in parallel from two control iPSC lines (11a, 18a), which were similar in their neuronal differentiation capacity, reprogramming method and donor age (Table S1). Differentiated preparations were plated on primary glial monolayers and the total number of ISL/TUJ1+ MNs was assessed after 3, 15 and 30 days in culture (Figure 1A-B). We found that in comparison to the number of MNs present in cultures made from each line at day 3, there was a trend towards a reduced number of *SOD1$^{+/A4V}$* MNs at 15 days (Figure S3A), which was further reduced and became statistically significant at day 30 (Figure 1C). Interestingly, we found no significant difference in the number of ISL-negative, TUJ1+, presumptive non-MNs between cases and controls at day 30 (Figure 1D).

To determine whether the selective decline in *SOD1$^{+/A4V}$* MN numbers was due to differential proliferation, we monitored progenitor activity via long-term BrdU incorporation (Figure S4). After chronic BrdU administration to cultures from day 0 to day 30, we found that only 2-3% of MNs were labeled (BrdU+, ISL+, TUJ1+) and that this modest rate of labeling was similar in both genotypes (Figure S4D-F). To confirm the effective labeling of

progenitors, we administered BrdU from day -17 of directed differentiation until day 0, finding that the vast majority of MNs (>95%) were BrdU+ (Figure S4A-C). These results suggest that the vast majority of MNs in our cultures were postmitotic prior to “day 0” and that the reduced *SOD1*$^{+/A4V}$ MN numbers were not due to a decrease in progenitor activity. Importantly, when we specifically quantified only the MNs born before day 0, we again found that significantly more *SOD1*$^{+/A4V}$ MNs were lost over the 30 days in culture (Figure 1E). In addition, at day 21, cultures from the two *SOD1*$^{+/A4V}$ cases exhibited an increase in TUNEL+ cells in compared to the two controls (Figure 1F), indicating an increased apoptotic rate. When we cultured control and patient derived MNs on primary glia from the *SOD1*$^{G93A}$ mouse model, we found that both genotypes of MNs survived significantly less than on control glia (Figure S3B). However, survival of *SOD1*$^{+/A4V}$ MNs was even lower than controls, suggesting a strong cell-autonomous contribution to the effects we observed.

The higher rate of apoptosis in *SOD1*$^{+/A4V}$ MNs was accompanied by altered morphological characteristics similar to those seen in patients and in the *SOD1*$^{G93A}$ mouse model (Kiernan and Hudson, 1991; McIlwain, 1991). In particular, 30-day old *SOD1*$^{+/A4V}$ MNs but not ISL-negative neurons, showed a significant reduction in relative soma size and fewer, as well as shorter processes compared to controls (Figure 1G-K and Figure S3C-F). MNs larger than 150μm$^2$ made up less than 40% of the total MN population in *SOD1*$^{+/A4V}$ cases, compared to ∼65% for controls (Figure 1K).

## Gene Targeting and Correction of the *SOD1*A4V Mutation

To determine whether the phenotypes we observed were dependent on the *SOD1*A4V allele, we used a two-step, zinc-finger nuclease (ZFN)-mediated gene targeting strategy to correct the mutation in iPSC line 39b (Figure 2A, methods). Gene-targeting and correction of *SOD1*A4V were confirmed through sequencing of a single PCR product amplified with primers outside the 5′ and 3′ homology arms, as well as through the elimination of a *Psh*A1 RFLP in the *SOD1* cDNA, which is specific to the mutant allele (Figure 2B-C and Figure S5A). Quantitative PCR demonstrated that the corrected 39b-*SOD1*$^{+/+}$ line did not harbor multiple insertions of the targeting vector, and that *SOD1* transcript levels were unchanged between the parental 39b-*SOD1*$^{+/A4V}$ and corrected cell lines (Figure 2D-E). We next examined SOD1 protein levels and found that while the intermediate 39b-*SOD1*$^{+/-}$ line, which expresses only one allele, exhibited approximately half of the SOD1 levels of the parental 39b-*SOD1*$^{+/A4V}$ cell line, correcting the mutation restored SOD1 protein levels (Figure 2F). As expected, based on the lower protein stability of the SOD1A4V variant (Cardoso et al., 2002), correction of the *SOD1* mutant allele resulted in a modest increase in SOD1 levels relative to the parental cells.

Given that undesired genetic variations could potentially arise as a result of ZFN off-target activity or clonal expansion, we carefully evaluated the genomic sequence and integrity of the parental and edited cell lines. We carried out whole genome sequencing for the 39b-*SOD1*$^{+/A4V}$ (33.4× coverage) and 39b-*SOD1*$^{+/+}$(31.1× coverage) cell lines, and determined that they closely matched each other throughout the genome for sequencing read depth (Figure S5B), excluding the possibility that large-scale copy-number variations (CNVs) had arisen during passaging, genome editing, or clonal expansion. This lack of large-scale CNVs

was validated using a lower resolution Nanostring nCounter Karyotyping Panel (Figure S5C). Moreover, the top 12,000 genomic loci with sequence similarity to the binding site of the ZFN pair we used, did not deviate between the two lines, indicating highly specific nuclease activity.

We also compared the fine-scale (SNP and indel) sequence calls between the two cell lines across their genomes. Overall, we found the corrected line to be free of such events. However, these analyses were sufficiently sensitive to identify a likely mitotic recombination event on the q arm of chr12 (from 108Mb to the end of the chromosome). Deeper analysis of this region demonstrated that the event had not induced novel or rare protein-coding variants. Neither had it induced coding variants associated with any known disease state, suggesting this event was likely to be phenotypically neutral. Analysis of the coding sequences of 26 genes implicated in ALS (Sreedharan and Brown, 2013), identified a single protein-altering difference, which corresponded to the genome edit of the A4V variant in *SOD1*.

Following the correction of the mutation, we used the 39b-$SOD1^{+/A4V}$ and 39b-$SOD1^{+/A4V}$ lines to ask whether the *SOD1*A4V-encoding variant was necessary for the MN survival and soma size phenotypes observed in the earlier patient-control comparisons. Importantly, correction of the mutation resulted in a significant rescue of both MN survival and soma size (Figure 2G-H).

## Solubility of Mutant SOD1 in Motor Neuron Cultures

SOD1 protein variants that cause ALS are prone to unfolding, misfolding and ultimately aggregation (Pasinelli and Brown, 2006). The pair of isogenic iPSC lines we developed allowed us to address the state of SOD1 in human MNs expressing physiological levels of this protein. Using immunoblotting assays on detergent-soluble and UREA fractions obtained from $SOD1^{+/+}$ and $SOD1^{+/A4V}$ MN cultures, we found no evidence of insoluble SOD1 protein under basal culture conditions (Figure 2I). Treatment with the proteasome inhibitor MG132, which increased soluble SOD1 levels 2-4 fold, resulted in the accumulation of detergent- insoluble SOD1 only in $SOD1^{+/A4V}$ neurons but not in isogenic controls (Figure 2I). In agreement with the biochemical analysis, aggregation of SOD1 was observed by immunocytochemistry only after treatment with MG132 and selectively in $SOD1^{+/A4V}$ MNs (Figure S6 C-E). Although we cannot rule out the possibility that undetectable levels of aggregated SOD1 protein were the cause of the degeneration of $SOD1^{+/A4V}$ MNs (Figure 1-2), our findings are consistent with recent claims that soluble mutant SOD1 can have substantial phenotypic effects (Brotherton et al., 2012).

## RNA sequencing of Purified $SOD1^{+/A4V}$ and Isogenic Control Motor Neurons

In order to gain insight into the molecular pathways affected by the *SOD1*A4V mutation in human MNs, we performed RNA sequencing. As in earlier experiments, we differentiated 39b-$SOD1^{+/A4V}$ and isogenic control iPSCs and plated them on a glial monolayer (Figure 3A). We next transduced these cultures with an *Hb9*: :RFP lentiviral reporter (Marchetto et al., 2008) and used FACS to purify MNs after 15 days of additional culture. We reasoned that at on day 15 we might identify the transcriptional changes that predisposed mature MNs

to apoptosis, as at this stage MNs were physiologically active (Figure S1 D-G), but there was only a trend towards reduced MN survival in *SOD1*$^{+/A4V}$ cultures (Figure S3A).

Unsupervised hierarchical clustering segregated samples based on their *SOD1* genotype, suggesting that effects of the mutant allele were driving measurable transcriptional differences between *SOD1*$^{+/A4V}$ and *SOD1*$^{+/+}$ MNs (Figure 3B). As a measure of the transcripts most affected by the *SOD1*A4V mutation we determined the identity of the 30 transcripts most increased and decreased in abundance at a false discovery rate (FDR) of 5% (Figure 3C, Table S2). Analysis of a representative subset of these genes by qRT-PCR in independent experiments validated our findings (Figure 3D). To understand whether the changes found by RNA-seq were specific to MNs and not present in cell types less affected in ALS we determined the expression of a subset of differentially expressed transcripts in the parental 39b and 39b corrected iPSCs (Figure S6A). Of 22 genes analyzed, only 19% were found to be differentially expressed in both iPSCs and MNs. Moreover, RNA-seq analysis on fibroblast cultures isolated from 5 healthy control individuals and the two ALS patients harboring the *SOD1*A4V mutation, failed to segregate transcriptomes based on genotype after unsupervised hierarchical clustering (Figure S6B). Importantly, a number of genes we identified to be misregulated in *SOD1*$^{+/A4V}$ MNs have not previously been implicated as being modulated by mutant SOD1 (Table S2).

## Ontology of Transcripts Modulated in *SOD1*$^{+/A4V}$ Motor Neurons

In order to probe the RNA-seq data for biological meaning we utilized two bioinformatic tools that query for enriched gene ontology terms (Table S3). We first performed gene-annotation enrichment analysis with DAVID (Huang da et al., 2009), using all the genes that were significantly altered (909 upregulated and 580 downregulated) in *SOD1*$^{+/A4V}$ MNs at a FDR of 5% (Table S3A-B). A total of 27 and 65 gene terms were enriched when increased and reduced transcripts were considered respectively. Transcripts implicated in ‘cytoskeleton’ organization, where amongst the most significantly induced in *SOD1*$^{+/A4V}$ MNs, consistent with the morphological alterations that we observed in these cells relative to isogenic controls (Figure 2H). Transcripts involved in ‘transcriptional regulation’ and ‘motor proteins’, were also induced as a result of the *SOD1* mutation. Amongst the significantly decreased transcripts in *SOD1*$^{+/A4V}$ MNs, there was a very strong enrichment for genes implicated in mitochondrial function and structure. In particular, 60% of all downregulated ontology terms were related to mitochondria, while genes implicated in ‘protein translation’ were also repressed (Table S3B).

As an alternative approach for querying our RNA-seq data, we performed Gene Set Enrichment Analysis (GSEA) (Mootha et al., 2003; Subramanian et al., 2005). GSEA identified 16 gene sets that were significantly induced in *SOD1*$^{+/A4V}$ MNs (NES<1.5; Table S3C). Amongst these gene sets, were the motor proteins ‘kinesins’. GSEA also identified 100 gene sets to be significantly repressed in *SOD1*$^{+/A4V}$ MNs (NES<1.5), and notably, gene sets associated with mitochondrial function and protein translation were again amongst the most significantly suppressed (Table S3D).

## *SOD1*$^{+/A4V}$ Motor Neurons Exhibit Disturbances in Mitochondrial Morphology and Motility

To determine whether the transcriptional changes in mitochondrial genes that we identified by RNA-seq in *SOD1*$^{+/A4V}$ MNs (Table S2-3) were indicative of actual disturbances to mitochondria, we initially performed electron microscopy (EM) studies (Figure 4B). Whereas mitochondrial morphology was normal in MNs derived from a control cell line (18a), mitochondria in *SOD1*$^{+/A4V}$ MNs (39b and RB9d) were commonly deranged and more vacuolar in appearance. These differences were mostly apparent in neuronal processes. We concluded that distortion in mitochondrial morphology was mediated by expression of the *SOD1*A4V mutant allele as correction of the mutation eliminated this phenotype (Figure 4B). To further validate mitochondrial damage in *SOD1*$^{+/A4V}$ MNs, we used immunoblotting assays to quantify the levels of two mitochondrial proteins, SDHA, which is encoded in the nucleus, and MT-COX1, encoded by mitochondrial DNA. We found that correction of the *SOD1*A4V allele in 39b-*SOD1*$^{+/+}$ MNs increased the protein levels of both SDHA and MT-COX1, relative to the parental 39b-*SOD1*$^{+/A4V}$ *MNs* (Figure 4C).

We next sought to measure the movements of mitochondria within the axons of our *in vitro*-derived MNs (Figure 4D-G). MN cultures differentiated from control and *SOD1*$^{+/A4V}$ iPSCs were co-labeled with *Hb9*::RFP and MitoTracker-Green, which selectively stained mitochondria. We then carried out live cell imaging to register mitochondrial movement along MN processes over the course of 5 minutes, and generated time/distance kymographs for further analysis (Figure 4D). We found that the A4V mutation resulted in a significant decrease in the number of motile mitochondria (Figure 4E). This was coupled to an increase in mitochondrial density in processes, as measured by the shorter distance between stationary mitochondria and the significantly smaller amount of space unoccupied by these organelles (Figure 4F, G).

## *SOD1*$^{+/A4V}$ Motor Neurons Exhibit Signatures of an Unfolded Protein Response (UPR) and ER Stress Induction

RNA-seq analysis showed that 93% of all transcripts involved in protein translation were reduced in *SOD1*$^{+/A4V}$ MNs (Figure 5A). Translational inhibition is a well-established hallmark of ER stress and the UPR, which is activated upon accumulation of misfolded proteins (Trusina et al., 2008). While the UPR is initially cytoprotective, its persistent activation can lead to apoptosis. In one of the branches of the pathway, pEIF2α leads to a global attenuation of translation and to selective translation of ATF4, while in another branch, IRE1 cleaves the mRNA of *XBP1*, creating its active spliced form (*sXBP1*) (Figure 5B) (Ron and Walter, 2007). The transcription factors, sXBP1 and ATF4 modulate expression of downstream effectors including chaperone proteins. Importantly, RNA-seq analysis identified the heat-shock proteins *DNAJC12* and *HSBP1*, the prefoldin subunits *PFDN2* and *PFDN5*, as well as the chaperonin subunits *CCT4* and *CCT7* as being differentially expressed in *SOD1*$^{+/A4V}$ MNs (Table S2). In addition, *SOD1*$^{+/A4V}$ MNs exhibited increased levels of pEIF2α (Figure 5C), as well as significantly elevated *sXBP1* transcript (Figure 5D) relative to isogenic controls, consistent with an active UPR.

To test if ER stress directly contributed to mutant SOD1-mediated toxicity in our culture system, we genetically manipulated the two UPR branches using siRNA knockdown of

*XBP1* and *ATF4* and assessed the effect on MN survival (Figure 5E, Figure S7B). Knockdown of *XBP1* resulted in a modest but significant increase in the number of $SOD1^{+/A4V}$ *MNs* after 30 days in culture (Figure 5F-G). In contrast, there was a trend for reduced MN numbers in the isogenic controls, suggesting that *XBP1* might provide a protective function in this context. Knockdown of *ATF4* depressed survival of both $SOD1^{+/A4V}$ and $SOD1^{+/+}$ MNs, implying that this protein plays a protective role in both contexts (Figure 5F). Given that reducing *ATF4* levels was detrimental to the survival of MNs we asked whether a further induction of pEIF2α would confer MN protection. Salubrinal is a selective inhibitor of phosphatases, which dephosphorylate pEIF2α (Boyce et al., 2005), and has previously been shown to extend the survival of the $SOD1^{G93A}$ mouse model (Saxena et al., 2009). To identify the optimal concentration for these experiments, we performed dose response treatments on FACS purified MNs and analyzed the expression of known UPR genes by qRT-PCR, leading to the selection of a 15μM concentration (Figure S6G). Treatment of cultures from d15-30 led to a modest but significant increase in the numbers of $SOD1^{+/A4V}$ MNs, whereas controls were not affected (Figure 5H).

## ER Stress is Inherent in Human Motor Neurons and Spinal Cord

Although the *SOD1*A4V mutation increased the levels of pEIF2α and of spliced *XBP1*, we noted that control MNs also expressed markers of an UPR, albeit at a lower level. This observation led us to hypothesize that MNs could be more sensitive to unfolded proteins and ER stress because the presence of these liabilities is a constitutive aspect of this neuronal sub-type's inherent biology. To test this, we compared the levels of *XBP1* splicing in purified, control HUES3 *Hb9*: :GFP+ MNs (Di Giorgio et al., 2008) with levels found in a range of other cell types including astrocytes, embryonic stem cells (ESCs), neural progenitors, fibroblasts, *Hb9*: :GFP-negative neurons and ESC-derived anterior neurons. Of all the cell types examined, only the control MNs displayed detectable levels of *sXBP1* that increased as MNs matured in culture (Figure 6A, S7A). When we compared the levels of *sXBP1* in RNA isolated from human brain and spinal cord (n=2; each replicate was pooled RNA from 22, non-overlapping, healthy controls), we strikingly saw little or no evidence in the brain, while in the spinal cord there was a marked and significant accumulation of the spliced transcript (Figure 6A, S7A).

We wondered whether this ongoing activation of the UPR pathway was associated with an increased sensitivity to ER-stress inducing agents such as DTT. Control MNs, indeed exhibited greater susceptibility to DTT administration than astrocytes and fibroblasts (Figure 6B). When we analyzed the area of the soma of MNs after treatment we found that the average soma size decreased substantially (Figure 6C), which given the acute nature of the treatment seemed most consistent with death of the largest MNs. These observations prompted us to investigate whether MN size correlated with basal ER stress levels. To address this, we purified *Hb9*: :RFP+ MNs and separated large and small populations (Figure 6D). We validated this approach by re-plating a subset of the purified MNs and measuring their soma size (Figure 6E). We then isolated RNA and examined the levels of *sXBP1* as an indicator of ER stress. Larger MNs showed significantly higher levels of *sXBP1* than smaller ones (Figure 6F) suggesting that an increased constitutive ER stress may contribute to their increased vulnerability in our cell-culture model.

## Inherent ER Stress in Human Motor Neurons is Dependent on Their Electrical Activity

Wainger and colleagues have found that the *SOD1*$^{+/A4V}$ human MNs that we report here are hyper-excitable in comparison to controls (Wainger et al., 2014). Given that the *XBP1* splicing levels increased as MNs matured in culture and became excitable (Figure 6A), we reasoned that a relationship might exist between the inherent ER stress we found in MNs and their electrophysiological activity. Treatment of MN cultures with sufficient tetrodotoxin (TTX) to effectively block action potentials (Figure S6C-D) significantly reduced spliced *XBP1* (Figure 6G). Reciprocally, treatment of cultures with the glutamatergic agonist kainate, which depolarizes MNs, led to a significant increase in spliced *XBP1* (Figure 6H). In addition, linopiridine, a compound that blocks Kv7 voltage gated potassium channels (Brown and Passmore, 2009), and increased MN activity (Figure S7D), also increased *XBP1* splicing (Figure 6H).

We next addressed the inverse question and assessed whether manipulating ER stress would affect the electrical activity of MNs. Treatment with salubrinal, resulted in a relative reduction in the number of spikes per minute (Figure 6I). Conversely, an acute treatment of MN cultures with DTT, which robustly induced *sXBP1* (Figure S6F), resulted in an increase in the number of spikes per minute (Figure 6J). These two data sets suggest that ER stress, the UPR and the physiological activity of human MNs are interconnected and that alterations in one of these pathways can affect the other (Figure 6K).

## A Subset of Transcriptional Changes in *SOD1*$^{+/A4V}$ are Shared in *C9orf72* MNs

A central question in the ALS field is whether mutations in the diverse causative genes converge on shared molecular pathways. To begin to address this question we focused on the most prevalent genetic ALS type and selected two familial patients (19, RB8) that carried *GGGGCC* repeat expansions in the *C9orf72* locus. We generated iPSCs, confirmed the presence of the expansion in both the parental fibroblasts as well as in multiple passages of the resulting iPSC lines and demonstrated the ability of these lines to differentiate into ISL/HB9+ MNs (Figure 7A-C, Table S1). To determine whether these MNs exhibited transcriptional disturbances similar to the ones that we identified in *SOD1*$^{+/A4V}$ MNs, we simultaneously differentiated them with six iPSC lines originating from five healthy individuals (Boulting et al., 2011) and FACS-purified *Hb9*: :RFP+ MNs in multiple biological replicates.

Using qRT-PCR we interrogated a subset of transcripts representative of pathways or cellular functions, which we had found to be altered by the *SOD1*A4V mutation (Figure 7D). Interestingly, in *C9orf72* mutant MNs, we did not detect a significant change in the transcript levels of genes implicated in electron transport in mitochondria, but we did detect a significant change in levels of the mitochondrial transporter *MTX3*. We also found a significant induction of catalase (*CAT*), indicative of oxidative stress. To determine whether intracellular transport might be impacted, we examined the two most highly upregulated motor proteins in *SOD1*$^{+/A4V}$ MNs and found that expression of the kinesin *KIF14* was significantly induced in *C9orf72* MNs. Finally, we analyzed the levels of 4 additional transcripts (*DNAJC12*, *EIF2B3*, *SCN1A*, *KCNN3*) to determine whether there was evidence for an unfolded protein response and/or shared changes in the expression of channels that

might be associated with changes in physiological activity. Of these transcripts, 3 of 4, including both cation channels and the protein chaperone *DNAJC12* were transcribed at significantly different levels between control and *C9orf72* MNs, supporting the notion that at least a subset of changes are shared between MNs of these two types.

Recently, Donnelly *et. al.*, reported transcriptional changes occurring in human iPSC-differentiated neurons from patients carrying either a *C9orf72* repeat expansion or an $SOD1^{+/D90A}$ mutant allele (Donnelly et al., 2013). We compared the transcriptional profile of our $SOD1^{+/A4V}$ mutant iPSC-derived MNs to these data sets by intersecting the respective gene lists. Of the 1,489 differentially expressed genes discovered in our $SOD1^{+/A4V}$ MNs, 357 were found to be misregulated in $SOD1^{+/D90A}$ neurons and 79 in the *C9orf72* expansion lines. This is consistent with the interpretation that *C9orf72* repeat expansions and *SOD1* mutations result in distinct but partially overlapping changes in transcript abundance.

## Discussion

Transgenic rodent models of ALS have been indispensable for developing hypotheses concerning how mutant SOD1 proteins induce MN degeneration. However, studies in these animals have yet to yield an effective treatment (Gladman et al., 2012). We reasoned that the gulf between successful animal studies and more positive clinical outcomes might be bridged with model systems that enable hypotheses originating from animals to be validated and extended in the context of human MNs bearing patient mutations. Utilizing iPSCs, genome editing and directed differentiation, we established a well-controlled cell culture system and interrogated the differential properties of patient-derived and healthy control MNs. Advances in gene targeting tools, which we have employed here, allowed our studies of the *SOD1*A4V variant to be elevated beyond correlative distinctions between ALS cases and controls to the demonstration of causal connections between this mutation and transcriptional as well as functional phenotypes.

Notably, our studies demonstrate that the *SOD1*A4V missense mutation was necessary to cause a pro-apoptotic phenotype in cultured human MNs, restricting their long-term survival. By employing RNA sequencing, we defined the transcriptional differences between human $SOD1^{+/A4V}$ and isogenic control MNs. Curating these data supported the view that patient-specific ALS iPSC-derived MNs display hallmarks of disease found in both patients and in animal models. We identified defects in mitochondrial transport and morphology, oxidative and ER-related stress and an activated UPR, all of which were dependent on the presence of the *SOD1*A4*V* mutation. Importantly, we also identified novel candidate genes, previously unstudied in the context of ALS, which were significantly affected by this disease-causing mutation. These newly identified genes will require further investigation as they may represent potential therapeutic targets. Our functional validation of the pathways in which these genes act suggest they will serve as an invaluable resource for many future studies of ALS.

We also found that other cell and neural-types were relatively unaffected by the *SOD1* mutation. As is observed in ALS patients, our molecular and pharmacological studies suggest that human MNs were more susceptible to mutant *SOD1*. We propose that this

susceptibility may originate from a pre-existing burden of ER stress that we found to be constitutively present in healthy, physiologically active MNs, but absent from a variety of other cell-types. Interestingly, this inherent ER stress positively correlated with MN size, drawing parallels to the fact that the largest α-MNs are the most vulnerable to degeneration in ALS patients (Kiernan and Hudson, 1991). It has previously been proposed that combinations of stressors may converge and reinforce each other leading to dysfunction and eventual degeneration of vulnerable neurons (Saxena and Caroni, 2011). We have found that the UPR, ER stress and electrical activity of MNs appear interconnected. Therefore distinct categories of compounds may be of substantial therapeutic benefit to ALS patients; those that support folding of proteins generally, those that specifically aid MNs in handling ER stress, and finally those that alter MN physiological activity. Our studies with salubrinal as well as those of Wainger and colleagues (Wainger et al., 2014) with retigabine, support this view. It is noteworthy that neither treatment with salubrinal, nor knockdown of *XBP1* alone resulted in a complete rescue of the survival deficit, implying that perhaps ER stress is only one of many components that contribute to MN death in our system.

While the function of the C9ORF72 protein remains unknown, the mechanism by which the hexanucleotide repeat expansion predisposes individuals to ALS has been suggested to range from haploinsufficiency to toxic gain-of-function properties of the mutant RNA or protein (Ash et al., 2013; DeJesus-Hernandez et al., 2011; Mori et al., 2013; Renton et al., 2011). Our studies indicate a partial conservation of transcriptional changes between *SOD1*$^{+/A4V}$ and *C9orf72* cases. Of particular note are transcripts reflecting a heightened oxidative stress response, reduced mitochondrial function, as well as changes in cation channels and motor proteins. Our discoveries of transcriptional and functional aberrations particularly in relation to mitochondria and ER stress in these patient-specific MNs could potentially relate to the typically late clinical onset of ALS, as these pathways are known to be involved in ageing. Taken together with the manuscript by Wainger et al. (Wainger et al., 2014), our work validates the utility of iPSCs and genome engineering strategies for probing relationships between the genetic variants responsible for ALS in the MNs that selectively degenerate in this disease.

## Experimental Procedures

### Cell culture

Stem cells were maintained on Matrigel (BD Biosciences) with mTeSR1 media (Stem Cell Technologies) and passaged by dispase (Gibco, 1mg/mL). All cell cultures were maintained at 37°C, 5% $CO^2$.

### Derivation of human fibroblasts and iPSC generation

Fibroblasts were generated from 3mm forearm dermal biopsies following informed consent as described previously (Dimos et al., 2008). Generation of iPSCs was done as reported previously by retroviral transduction of *KLF4*, *SOX2*, *OCT4* and *(cMYC)* (Boulting et al., 2011).

### Motor neuron differentiation

MNs differentiation was carried out as previously described (Boulting et al., 2011) with a few modifications (see also Figure S1). Briefly, iPSC colonies were dissociated to single cells with accutase and plated in suspension in low-adherence flasks, at a 400K/ml density with 10μM ROCK inhibitor (Sigma) in mTeSR1 media for 24hrs. Embryoid bodies (EBs) were formed and media was gradually diluted (50% on day 3 and 100% on day 4) to KOSR (DMEM/F12, 15% KOSR) between days 1-4 and to a neural induction medium (NIM: DMEM/F12 with L-glutamine, NEAA, Heparin (2μg/ml), N2 supplement (Gibco) for days 5-24. Treatment with small molecules and recombinant proteins was as follows: on d1-d6, 10μM SB431542 (Sigma) + 1μM Dorsmorphin (Stemgent); on d5-d24 10ng/mL BDNF (R&D), 0.4μg/ml ascorbic acid (AA, Sigma), 1μM Retinoic Acid (RA, Sigma) and 1μM Smoothened Agonist 1.3 (SAG 1.3, Calbiochem). At day 24 EBs were dissociated to single cells with Papain/DNase (Worthington Bio) and plated onto lysine/laminin-coated surfaces (BD Biosciences) for relevant experiments.

### Motor neuron survival assay

20K differentiated MN cultures were plated on 8-well chamber slides (BD biosciences) containing a confluent monolayer of primary cortical mouse glia. Primary glial preparations from P0-P2 mouse pups were obtained as described previously (Di Giorgio et al., 2008). Co-cultures were maintained in Neurobasal media (NB, Invitrogen), supplemented with B27 and N2 supplement (Gibco), 10ng/mL of each of BDNF, GDNF, CNTF (R&D) and 0.4μg/ml ascorbic acid (Sigma) and fed every 2-3 days. Slides were fixed at various time points, cultures were stained and cell numbers assessed. Whole-well images were quantified in a manner blinded to the genotype and condition of the experiment. Neuronal numbers on day 3 were set as 100% and numbers on subsequent time points were expressed as a percentage of day 3. To evaluate cell death, neuronal cultures were plated without glia on coverslips and live cells were assayed using the In Situ Cell Death Kit (Roche Diagnostics) according to manufacturer's instructions.

### Electrophysiology recordings

MNs were plated at 20K cells/$cm^2$ on coverslips, in the presence of primary mouse glia and allowed to mature for 2-4 weeks. MNs were identified by RFP fluorescence, after transduction with the *Hb9*: :RFP lentivirus (Marchetto et al., 2008). Whole-cell voltage-clamp or current-clamp recordings were made using a Multiclamp 700B (Molecular Devices). Data were digitized with a Digidata 1440A A/D interface and recorded using pCLAMP 10_software (Molecular Devices). For MEA recordings, equal numbers of MN cultures were plated on lysine/laminin coated M768-GLx 12-well plates (Axion BioSystems) at typical densities of 40-80K/well and recorded after approximately 14 days using an Axion Maestro device and analyzed using Axion Integrated Studio software.

### RNA preparation, qRT-PCR and RNA-seq

RFP+ MNs for RNA assays were purified by FACS 8-10 days after transduction with *Hb9*: :RFP lentiviral reporter, following a total of 15 days of co-culture with mouse glia. Total RNA was isolated using Trizol LS (Invitrogen) according to manufacturer's

instructions. A total of 300-1000ng was used to synthesize cDNA by reverse transcription according to the iSCRIPT kit (Bio-Rad). qRT-PCR was then performed using SYBR green (Bio-Rad) and the iCycler system (Bio-Rad). Quantitative levels for all genes were normalized to the average levels of 3 housekeeping genes (*GAPDH/β-Actin/YWHAZ*) and expressed relative to the relevant control samples or the lowest expressing sample in the experiment. For RNA-Seq, libraries were generated from ~250ng total RNA using the illumina TruSeq RNA kit v2, according to the manufacturer's directions. Libraries were sequenced at the Harvard Bauer Core Sequencing facility on a HiSeq 2000. All FASTQ files were analyzed using FastQC software (v 0.10.1) to confirm that Phred scores were acceptable at all read positions (median Phred score>25 and lower quartile>20). The FASTQ files were aligned to the GRCh37/hg19 reference genome using Tophat (v 2.0.7). Data analysis was performed by DSeq, GEO submission number for RNA-seq is GSE54409.

## Mitochondrial transport assays and EM analysis

*Hb9*: :RFP+ MNs were stained with 50nM MitoTracker® Green FM (Invitrogen) and transferred to a custom observation chamber mounted on the stage of a Nikon Eclipse Ti microscope equipped with an automated stage and In Vivo Scientific incubator. Mitochondrial movements were recorded for 5 minutes with 4-second time-lapse intervals using NIS-Elements (Nikon) using a 63× lens. Kymographs were generated from each video using NIS-Elements Analyzing Software (Nikon). Mitochondria were considered motile if they traveled faster than 0.017 μm/second. For Electron Microscopy analysis, ~60nm thick sections of MN cultures were fixed with 2.5% glutaraldehyde-2% paraformaldehyde in 0.1M sodium cacodylate buffer (pH 7.4) and maintained at 4°C O/N. Following post-fixing, cells were then embedded in plastic and ~60nm thick sections were cut, stained with lead citrate and analyzed in a JEOL 1200EX Transmission Electron Microscope. At least 3 independent differentiation experiments were analyzed in each case and pictures were taken by a technician blinded for sample IDs.

## *XBP1* splicing assay

300ng of RNA was used to generate cDNA. PCR products were analyzed after electrophoresis on a 2% low-melting agarose gel. The ratio of spliced/unspliced bands was quantified using Image J software.

## Gene targeting

Zinc finger nucleases (ZFNs) targeting the *SOD1* locus were constructed using a modified version of the OPEN method (Maeder et al., 2008) and their nuclease activity was validated in HEK293 cells. For genetic correction of 39b-$SOD1^{+/A4V}$ iPSC line, 2.5 million cells were nucleofected (Amaxa™) with 1 μg of ZFN plasmid and 5μg of targeting plasmid. 48hrs after, puromycin selection was applied for 1 week. Surviving colonies were expanded and PCR was used to confirm proper targeting. To remove the puromycin cassette from the intermediate $SOD1^{+/-}$ cells, 2.5 million cells were nucleofected with 5μg of a mammalian expression plasmid containing the FLp recombinase. Sequencing of the genomic DNA was used to confirm removal of the puromycin cassette. Copy number qPCR was performed as described previously (D'Haene et al., 2010) to rule out random integration events.

## Genome sequencing and analysis

DNA samples were obtained from the parental 39b-*SOD1*$^{+/A4V}$ cell line and the gene corrected clone using phenol chloroform extraction. The sequencing libraries were made with 50ng of genomic DNA using the Illumina Nexterra DNA kit. Deep (30×) WGS was performed using the Illumina HiSeq 2500 Platform (500 bp library, 101 bp reads). All subsequent alignments and analysis were performed with hg19 as a reference. To investigate whether there were changes in copy number we used Genome STRiP (Handsaker et al., NG, 2011). To look for regions of copy number change, we evaluated the ratio of normalized read depth in the derived cell line compared to the parental cell line in each window. To find rare coding SNPs in ALS genes, we annotated coding variants called by Haplotype caller with SNPeff (Abecasis et al., 2012). SNPs classified as missense, silent, or nonsense were retained. We then integrated allele frequencies for the European population from the thousand genomes project (Cingolani et al., 2012). Variants were selected that overlapped target genes for ALS. To find variants that differed between cell lines, we compared the genotypes of both lines in a stringent manner similar to the methodologies used to discover *de novo* mutations. To examine the off-target effects of the designed nuclease, variants within the top 12,000 potential off-target nuclease cut sites were selected from this filtered set of confident variants.

## Immunocytochemistry

Cell cultures were fixed in 4% PFA for 15 minutes at 4°C, permeabilized with 0.2% Triton-X in PBS for 45 minutes and blocked with 10% donkey serum in PBS-T (Triton 0.1%). Cells were then incubated in primary antibody overnight and in secondary antibodies for 1 hour in 2% donkey serum in PBS-T after several washes in between. See supplemental methods for a full list of antibodies.

## Western Blot assays

For analysis of Phospho-eIF2α protein, cells were lysed in RIPA buffer with protease and phosphatase inhibitors (Roche). 20μg of protein were separated by SDS-PAGE and transferred to nitrocellulose membranes. Anti-Phospho-eIF2α (#3597, Cell Signaling Technology), anti-α–Tubulin (abcam, ab4074) and anti-eIF2α (Cell Signaling Technology, #9722) antibodies were used. For SOD1 protein, detergent-soluble (RIPA buffer) and detergent-insoluble (UREA buffer) fractions were obtained and 5μg of protein samples were separated by SDS-PAGE, transferred to PDVF membranes and probed with anti-SOD1 (Agrisera #AS09 540) and anti-α–Tubulin (Sigma Aldrich # T6199). For mitochondrial biogenesis analysis, 6μg of protein samples were analyzed using the MitoBiogenesis™ Western Blot Cocktail (ab123545).

## Statistical analysis

Statistical significance was assessed by a standard Student's T test (1 tail & 2 tail); $P<0.05$ was considered significant. Two-tailed, unpaired tests were used except to confirm specific hypotheses, in which case one-tailed, unpaired tests were used.

## Supplementary Material

Refer to Web version on PubMed Central for supplementary material.

## Acknowledgments

We thank H. Mitsumoto and D. McKenna-Yasek for performing skin biopsies. K. Koszka for maintaining mice; all members of the Eggan Lab, C. Henderson and MW. Amoroso for helpful comments on the manuscript. RHB acknowledges generous support from the ALS Therapy Alliance, Project ALS, P2ALS, the Angel Fund, the Pierre L. de Bourgknecht ALS Research Foundation, the Al-Athel ALS Research Foundation, the ALS Family Charitable Foundation and the NIH/NINDS (1R01NS050557 and NINDS ARRA Award RC2-NS070-342). This work was funded by Target ALS, Project A.L.S., P2ALS, NINDS GO grant (5RC2NS069395-02), NINDS R24 (1U24NS078736-01), HHMI and NIH Director's Pioneer Award DP1 (OD006862). E.K. is a Charles A. King Trust Postdoctoral fellow; K.E. is an HHMI early career scientist.

## References

Abecasis GR, Auton A, Brooks LD, DePristo MA, Durbin RM, Handsaker RE, Kang HM, Marth GT, McVean GA. An integrated map of genetic variation from 1,092 human genomes. Nature. 2012; 491:56–65. [PubMed: 23128226]

Ash PE, Bieniek KF, Gendron TF, Caulfield T, Lin WL, Dejesus-Hernandez M, van Blitterswijk MM, Jansen-West K, Paul JW 3rd, Rademakers R, et al. Unconventional translation of C9ORF72 GGGGCC expansion generates insoluble polypeptides specific to c9FTD/ALS. Neuron. 2013; 77:639–646. [PubMed: 23415312]

Bilican B, Serio A, Barmada SJ, Nishimura AL, Sullivan GJ, Carrasco M, Phatnani HP, Puddifoot CA, Story D, Fletcher J, et al. Mutant induced pluripotent stem cell lines recapitulate aspects of TDP-43 proteinopathies and reveal cell-specific vulnerability. Proc Natl Acad Sci U S A. 2012; 109:5803–5808. [PubMed: 22451909]

Boulting GL, Kiskinis E, Croft GF, Amoroso MW, Oakley DH, Wainger BJ, Williams DJ, Kahler DJ, Yamaki M, Davidow L, et al. A functionally characterized test set of human induced pluripotent stem cells. Nat Biotechnol. 2011; 29:279–286. [PubMed: 21293464]

Boyce M, Bryant KF, Jousse C, Long K, Harding HP, Scheuner D, Kaufman RJ, Ma D, Coen DM, Ron D, et al. A selective inhibitor of eIF2alpha dephosphorylation protects cells from ER stress. Science. 2005; 307:935–939. [PubMed: 15705855]

Brotherton TE, Li Y, Glass JD. Cellular toxicity of mutant SOD1 protein is linked to an easily soluble, non-aggregated form in vitro. Neurobiol Dis. 2012; 49C:49–56. [PubMed: 22926189]

Brown DA, Passmore GM. Neural KCNQ (Kv7) channels. Br J Pharmacol. 2009; 156:1185–1195. [PubMed: 19298256]

Cardoso RM, Thayer MM, DiDonato M, Lo TP, Bruns CK, Getzoff ED, Tainer JA. Insights into Lou Gehrig's disease from the structure and instability of the A4V mutant of human Cu,Zn superoxide dismutase. J Mol Biol. 2002; 324:247–256. [PubMed: 12441104]

Cingolani P, Platts A, Wang le L, Coon M, Nguyen T, Wang L, Land SJ, Lu X, Ruden DM. A program for annotating and predicting the effects of single nucleotide polymorphisms, SnpEff: SNPs in the genome of Drosophila melanogaster strain w1118; iso-2; iso-3. Fly. 2012; 6:80–92. [PubMed: 22728672]

D'Haene B, Vandesompele J, Hellemans J. Accurate and objective copy number profiling using real-time quantitative PCR. Methods. 2010; 50:262–270. [PubMed: 20060046]

DeJesus-Hernandez M, Mackenzie IR, Boeve BF, Boxer AL, Baker M, Rutherford NJ, Nicholson AM, Finch NA, Flynn H, Adamson J, et al. Expanded GGGGCC hexanucleotide repeat in noncoding region of C9ORF72 causes chromosome 9p-linked FTD and ALS. Neuron. 2011; 72:245–256. [PubMed: 21944778]

Di Giorgio FP, Boulting GL, Bobrowicz S, Eggan KC. Human embryonic stem cell-derived motor neurons are sensitive to the toxic effect of glial cells carrying an ALS-causing mutation. Cell Stem Cell. 2008; 3:637–648. [PubMed: 19041780]

Dimos JT, Rodolfa KT, Niakan KK, Weisenthal LM, Mitsumoto H, Chung W, Croft GF, Saphier G, Leibel R, Goland R, et al. Induced pluripotent stem cells generated from patients with ALS can be differentiated into motor neurons. Science. 2008; 321:1218–1221. [PubMed: 18669821]

Donnelly CJ, Zhang PW, Pham JT, Heusler AR, Mistry NA, Vidensky S, Daley EL, Poth EM, Hoover B, Fines DM, et al. RNA toxicity from the ALS/FTD C9ORF72 expansion is mitigated by antisense intervention. Neuron. 2013; 80:415–428. [PubMed: 24139042]

Egawa N, Kitaoka S, Tsukita K, Naitoh M, Takahashi K, Yamamoto T, Adachi F, Kondo T, Okita K, Asaka I, et al. Drug screening for ALS using patient-specific induced pluripotent stem cells. Sci Transl Med. 2012; 4:145ra104.

Gladman M, Cudkowicz M, Zinman L. Enhancing clinical trials in neurodegenerative disorders: lessons from amyotrophic lateral sclerosis. Curr Opin Neurol. 2012; 25:735–742. [PubMed: 23160423]

Gurney ME, Pu H, Chiu AY, Dal Canto MC, Polchow CY, Alexander DD, Caliendo J, Hentati A, Kwon YW, Deng HX, et al. Motor neuron degeneration in mice that express a human Cu,Zn superoxide dismutase mutation. Science. 1994; 264:1772–1775. [PubMed: 8209258]

Hardiman O, van den Berg LH, Kiernan MC. Clinical diagnosis and management of amyotrophic lateral sclerosis. Nat Rev Neurol. 2011; 7:639–649. [PubMed: 21989247]

Howland DS, Liu J, She Y, Goad B, Maragakis NJ, Kim B, Erickson J, Kulik J, DeVito L, Psaltis G, et al. Focal loss of the glutamate transporter EAAT2 in a transgenic rat model of SOD1 mutant-mediated amyotrophic lateral sclerosis (ALS). Proc Natl Acad Sci U S A. 2002; 99:1604–1609. [PubMed: 11818550]

Huang da W, Sherman BT, Lempicki RA. Systematic and integrative analysis of large gene lists using DAVID bioinformatics resources. Nat Protoc. 2009; 4:44–57. [PubMed: 19131956]

Kiernan JA, Hudson AJ. Changes in sizes of cortical and lower motor neurons in amyotrophic lateral sclerosis. Brain. 1991; 114(Pt 2):843–853. [PubMed: 2043953]

Maeder ML, Thibodeau-Beganny S, Osiak A, Wright DA, Anthony RM, Eichtinger M, Jiang T, Foley JE, Winfrey RJ, Townsend JA, et al. Rapid “open-source” engineering of customized zinc-finger nucleases for highly efficient gene modification. Mol Cell. 2008; 31:294–301. [PubMed: 18657511]

Marchetto MC, Muotri AR, Mu Y, Smith AM, Cezar GG, Gage FH. Non-cell-autonomous effect of human SOD1 G37R astrocytes on motor neurons derived from human embryonic stem cells. Cell Stem Cell. 2008; 3:649–657. [PubMed: 19041781]

McIlwain DL. Nuclear and cell body size in spinal motor neurons. Adv Neurol. 1991; 56:67–74. [PubMed: 1853783]

Mootha VK, Bunkenborg J, Olsen JV, Hjerrild M, Wisniewski JR, Stahl E, Bolouri MS, Ray HN, Sihag S, Kamal M, et al. Integrated analysis of protein composition, tissue diversity, and gene regulation in mouse mitochondria. Cell. 2003; 115:629–640. [PubMed: 14651853]

Mori K, Weng SM, Arzberger T, May S, Rentzsch K, Kremmer E, Schmid B, Kretzschmar HA, Cruts M, Van Broeckhoven C, et al. The C9orf72 GGGGCC Repeat Is Translated into Aggregating Dipeptide-Repeat Proteins in FTLD/ALS. Science. 2013

Oh YK, Shin KS, Yuan J, Kang SJ. Superoxide dismutase 1 mutants related to amyotrophic lateral sclerosis induce endoplasmic stress in neuro2a cells. J Neurochem. 2008; 104:993–1005. [PubMed: 18233996]

Pasinelli P, Brown RH. Molecular biology of amyotrophic lateral sclerosis: insights from genetics. Nat Rev Neurosci. 2006; 7:710–723. [PubMed: 16924260]

Renton AE, Majounie E, Waite A, Simon-Sanchez J, Rollinson S, Gibbs JR, Schymick JC, Laaksovirta H, van Swieten JC, Myllykangas L, et al. A hexanucleotide repeat expansion in C9ORF72 is the cause of chromosome 9p21-linked ALS-FTD. Neuron. 2011; 72:257–268. [PubMed: 21944779]

Robberecht W, Philips T. The changing scene of amyotrophic lateral sclerosis. Nat Rev Neurosci. 2013; 14:248–264. [PubMed: 23463272]

Ron D, Walter P. Signal integration in the endoplasmic reticulum unfolded protein response. Nat Rev Mol Cell Biol. 2007; 8:519–529. [PubMed: 17565364]

Rosen DR, Siddique T, Patterson D, Figlewicz DA, Sapp P, Hentati A, Donaldson D, Goto J, O'Regan JP, Deng HX, et al. Mutations in Cu/Zn superoxide dismutase gene are associated with familial amyotrophic lateral sclerosis. Nature. 1993; 362:59–62. [PubMed: 8446170]

Sareen D, O'Rourke JG, Meera P, Muhammad AK, Grant S, Simpkinson M, Bell S, Carmona S, Ornelas L, Sahabian A, et al. Targeting RNA foci in iPSC-derived motor neurons from ALS patients with a C9ORF72 repeat expansion. Sci Transl Med. 2013; 5:208ra149.

Saxena S, Cabuy E, Caroni P. A role for motoneuron subtype-selective ER stress in disease manifestations of FALS mice. Nat Neurosci. 2009; 12:627–636. [PubMed: 19330001]

Saxena S, Caroni P. Selective neuronal vulnerability in neurodegenerative diseases: from stressor thresholds to degeneration. Neuron. 2011; 71:35–48. [PubMed: 21745636]

Sreedharan J, Blair IP, Tripathi VB, Hu X, Vance C, Rogelj B, Ackerley S, Durnall JC, Williams KL, Buratti E, et al. TDP-43 mutations in familial and sporadic amyotrophic lateral sclerosis. Science. 2008; 319:1668–1672. [PubMed: 18309045]

Sreedharan J, Brown RH Jr. Amyotrophic lateral sclerosis: Problems and prospects. Ann Neurol. 2013

Subramanian A, Tamayo P, Mootha VK, Mukherjee S, Ebert BL, Gillette MA, Paulovich A, Pomeroy SL, Golub TR, Lander ES, et al. Gene set enrichment analysis: a knowledge-based approach for interpreting genome-wide expression profiles. Proc Natl Acad Sci U S A. 2005; 102:15545–15550. [PubMed: 16199517]

Trusina A, Papa FR, Tang C. Rationalizing translation attenuation in the network architecture of the unfolded protein response. Proc Natl Acad Sci U S A. 2008; 105:20280–20285. [PubMed: 19075238]

Wada T, Goparaju SK, Tooi N, Inoue H, Takahashi R, Nakatsuji N, Aiba K. Amyotrophic lateral sclerosis model derived from human embryonic stem cells overexpressing mutant superoxide dismutase 1. Stem Cells Transl Med. 2012; 1:396–402. [PubMed: 23197818]

Wainger B, Kiskinis E, Mellin C, Wiskow O, Han S, Sandoe J, Perez N, Williams L, Lee S, Boulting G, et al. Intrinsic Membrane Hyperexcitability of ALS Patient-Derived Motor Neurons. Cell Reports. 2014

## Highlights

- iPSC-derived motor neurons harboring *SOD1* mutations exhibit cell survival deficits
- Genetic correction rescues ALS-related phenotypes
- RNA-seq reveals novel expression changes, mitochondrial and ER stress disturbances
- MNs exhibit inherent ER stress linked to electrical activity

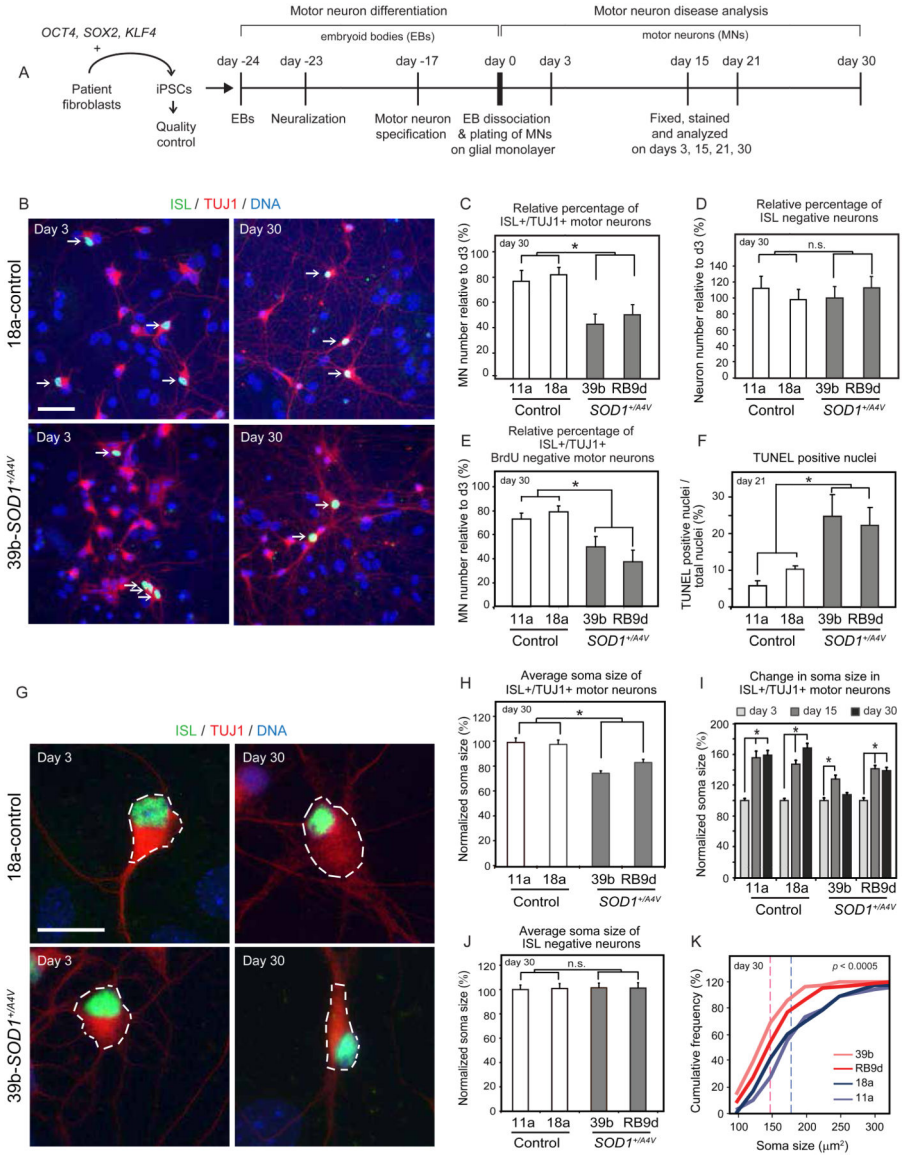


**Figure 1. iPSC-Derived Motor Neurons From *SOD1*$^{+/A4V}$ ALS Patients Exhibit Survival and Morphometric Differences Relative to Healthy Controls**

**(A)** Experimental outline: patient fibroblasts were reprogrammed to generate iPSCs, which were differentiated into MNs and assessed for ALS-related phenotypes. (**B**) Neuronal cultures on glial monolayers 3 and 30 days post-differentiation from control and *SOD1*$^{+/A4V}$ iPSCs. MNs co-stained for ISL and TUJ1 are indicated by white arrows (scale bar=50μm). (**C**) Quantifications of ISL positive MNs (n=3, m>8000, +/-SEM, P<0.05), and (**D**) ISL negative neurons (n=3, m>25000, +/-SEM, P<0.05), after 30 days in culture. (**E**) Quantifications of MN numbers that are BrdU negative after 30 days in culture (n=1, m>3600, +/-SD, P<0.05). Differential motor neurogenesis does not explain the lower numbers in *SOD1*$^{+/A4V}$ cases. (**F**) Quantifications of TUNEL positive nuclei of neuronal cultures without glia after 21 days in culture, (n=2, m>13000, +/-SD, P<0.05). (**G**) Representative images of measured soma size (white-dotted circumference) of control and *SOD1*$^{+/A4V}$ MNs, (scale bar=20μm). (**H**) Quantifications of ISL positive MN soma size,

values normalized to controls (n=3, m=340, +/-SEM, P<0.01). (**I**) MN soma size after 3, 15 and 30 days in culture normalized to day 3 for each cell line. Although MNs increase in size over time in all 4 cell lines, they do less so in *SOD1*$^{+/A4V}$ cases. (**J**) Quantifications of ISL negative neuron soma size, values normalized to controls (n=3, m=446, +/-SEM, P: n.s.). (**K**) Cumulative frequency graphs of MN soma size after 30 days in culture. Dotted lines indicate averages for control and disease. n.s: not significant; n=experiment, m=cell number.

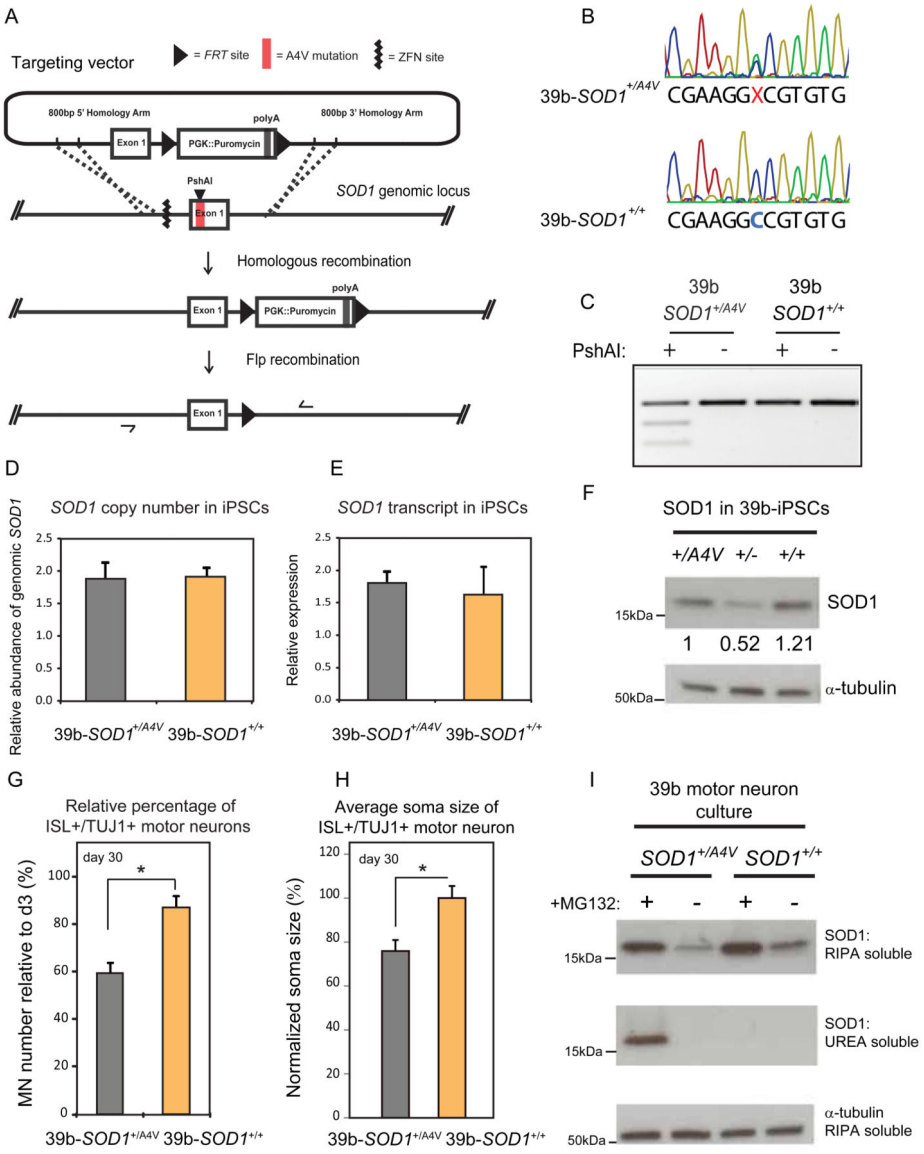


**Figure 2. Genetic Correction of the *SOD1A4V* Mutant Allele Rescues Motor Neuron Survival and Soma Size Deficits**

**(A)** Gene targeting strategy used to generate isogenic 39b-*SOD1*$^{+/+}$ iPSC line. Nucleases targeting the *SOD1* locus created a double strand break upstream of *Exon*1; homologous recombination of the genomic locus with a targeting plasmid with control sequence of *Exon*1 coupled to *PGK::Puromycin* replaced the *SOD1A4V* mutant allele; after antibiotic selection, the resistance cassette was removed by Flp-mediated recombination, leaving only an *FRT* footprint.; ZFN: Zinc Finger Nuclease, FRT: Flippase Recognition Target. (**B**) Sequencing chromatograms of *Exon*1 of *SOD1* in iPSC line 39b before and after targeting, demonstrate the correction of the A4V mutation. (**C**) *Psh*AI restriction digestion of amplified *SOD1* cDNA before and after gene targeting. The mutation creates a *PshAI* restriction site that is absent in the corrected line. (**D**) qPCR of genomic *SOD1* shows that there are no extra copies of the gene in the corrected line and (**E**) qRT-PCR of cDNA shows that the expression levels of *SOD1* are the same in the corrected line (n=3, +/-SEM). (**F**)

SOD1 protein levels assessed by western blot (WB) analysis in parental (39b-*SOD1*$^{+/A4V}$), targeted hemizygous knockout (39b-*SOD1*$^{+/-}$) and corrected (39b-*SOD1*$^{+/+}$) iPSC clones. (**G**) Isogenic 39b-*SOD1*$^{+/+}$ MNs exhibit increased cell survival (n=6, m>13000, +/-SEM, P<0.05) and (**H**) soma size (n=3, m=280, +/-SEM, P<0.01). (**I**) WB analysis of SOD1 protein in detergent- soluble (RIPA) and detergent-insoluble (UREA) fractions in day 12 neuronal cultures. Insoluble SOD1 is not detected under normal conditions. After proteasome inhibition by MG132 treatment, insoluble SOD1 selectively accumulates only in *SOD1*$^{+/A4V}$ MNs and not in the corrected line.

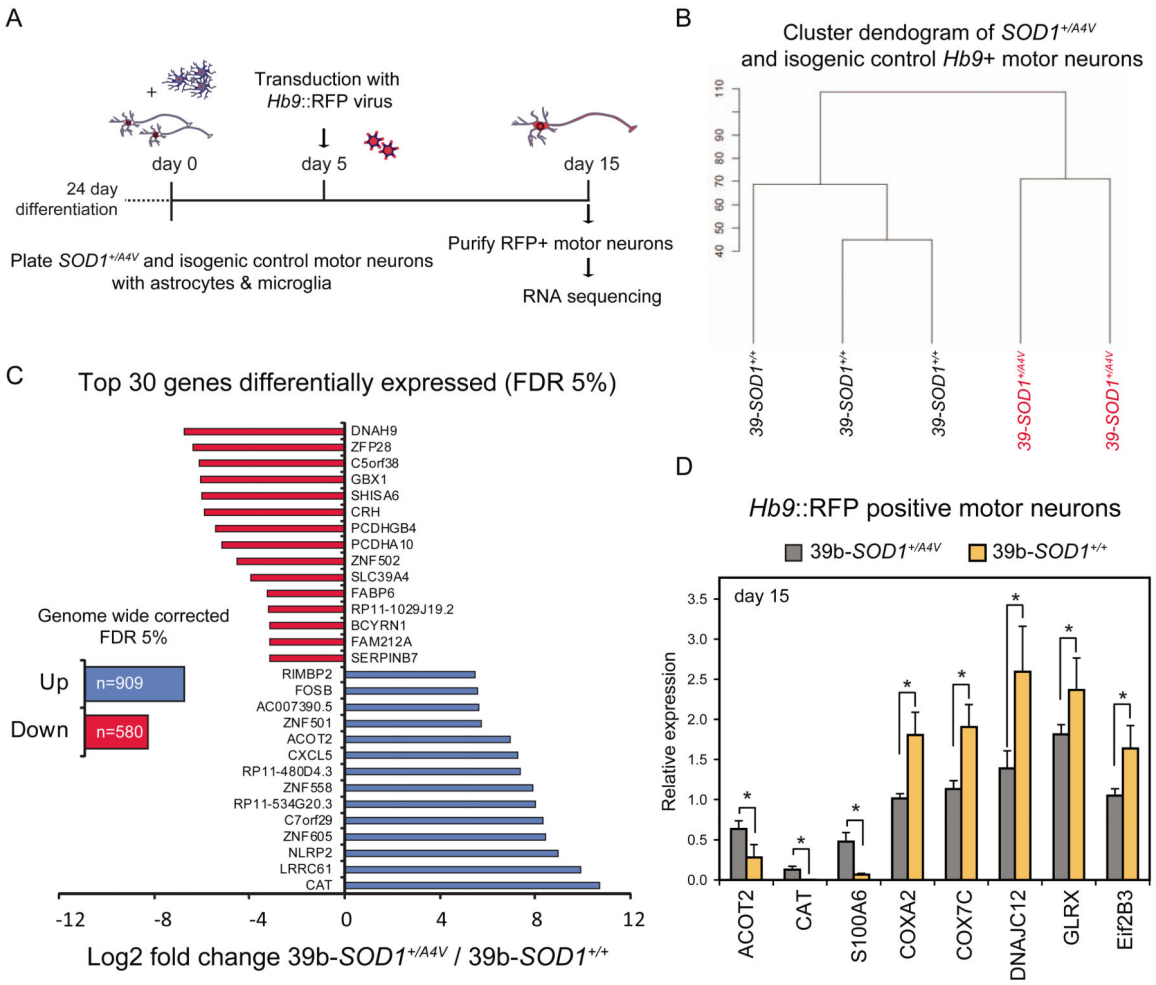


**Figure 3. Transcriptional Analysis of 39b-*SOD1*$^{+/A4V}$ and Isogenic Control Motor Neurons by RNA-Seq Reveals Genotypic Regulatory Changes**

**(A)** Experimental outline: *SOD1*$^{+/A4V}$ and isogenic control MN cultures were co-cultured with primary glial cells, transduced with an *Hb9*: :RFP lentivirus and FACS-purified on day 15 for RNA isolation and sequencing. (**B**) Dendogram demonstrating clear genotypic clustering based on transcriptional changes measured by RNA sequencing. (**C**) Total number of genes and top 30 genes (based on fold change) misregulated in *SOD1*$^{+/A4V}$ MNs with an FDR 5%. (**D**) qRT-PCR validation of misregulated genes in independent samples (n=3, +/-SEM).

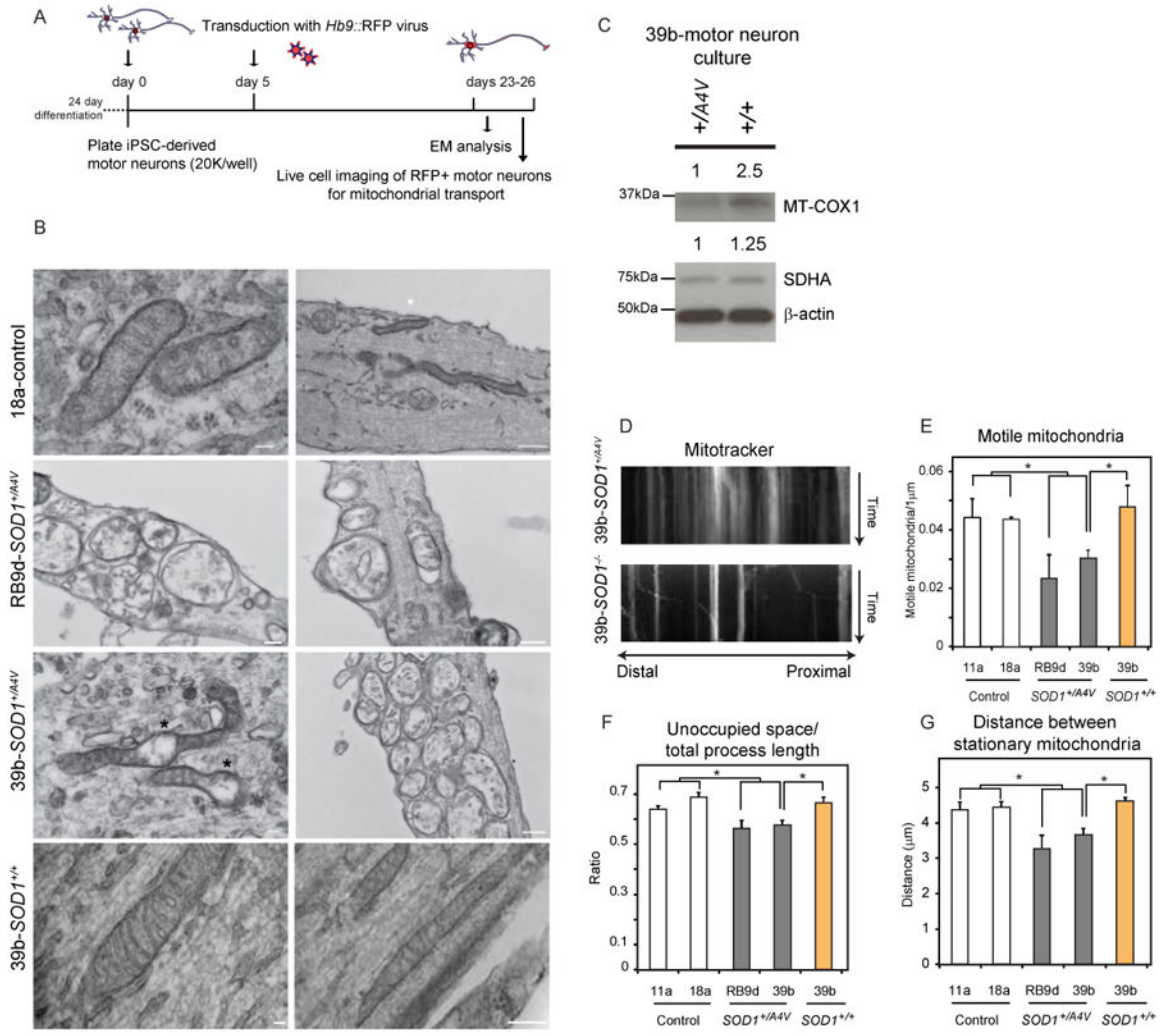


**Figure 4. *SOD1*$^{+/A4V}$ Motor Neurons Exhibit Mitochondrial Defects That are Rescued by Genetic Correction of the *SOD1*A4V Mutation**

**(A)** Experimental outline: *SOD1*$^{+/A4V}$ and isogenic control MN cultures were plated at low densities, transduced with an *Hb9*::RFP lentivirus on day 5 and analyzed on days 23-26. (**B**) Electron microscopy analysis demonstrating that in contrast to control neurons (top panel), *SOD1*$^{+/A4V}$ neurons (middle panels) often exhibited swelling, morphological disorganization and clustering in neurites. Mitochondria in genetically corrected neurons (bottom panel) exhibited normal morphological characteristics. Representative images out of 3 independent experiments are shown. (**C**) WB analysis of mitochondrial proteins. (**D**) Representative kymographs of MitoTracker-stained mitochondria in MNs after live cell imaging. Distal and proximal orientation relative to cell body is indicated. *SOD1*$^{+/A4V}$ MNs exhibit mitochondria transportation deficiencies relative to controls with (**E**) fewer motile mitochondria, (**F**) less space unoccupied by mitochondria relative to axon length and (**G**) shorter distances between stationary mitochondria (n=4, +/-SEM, P<0.05).

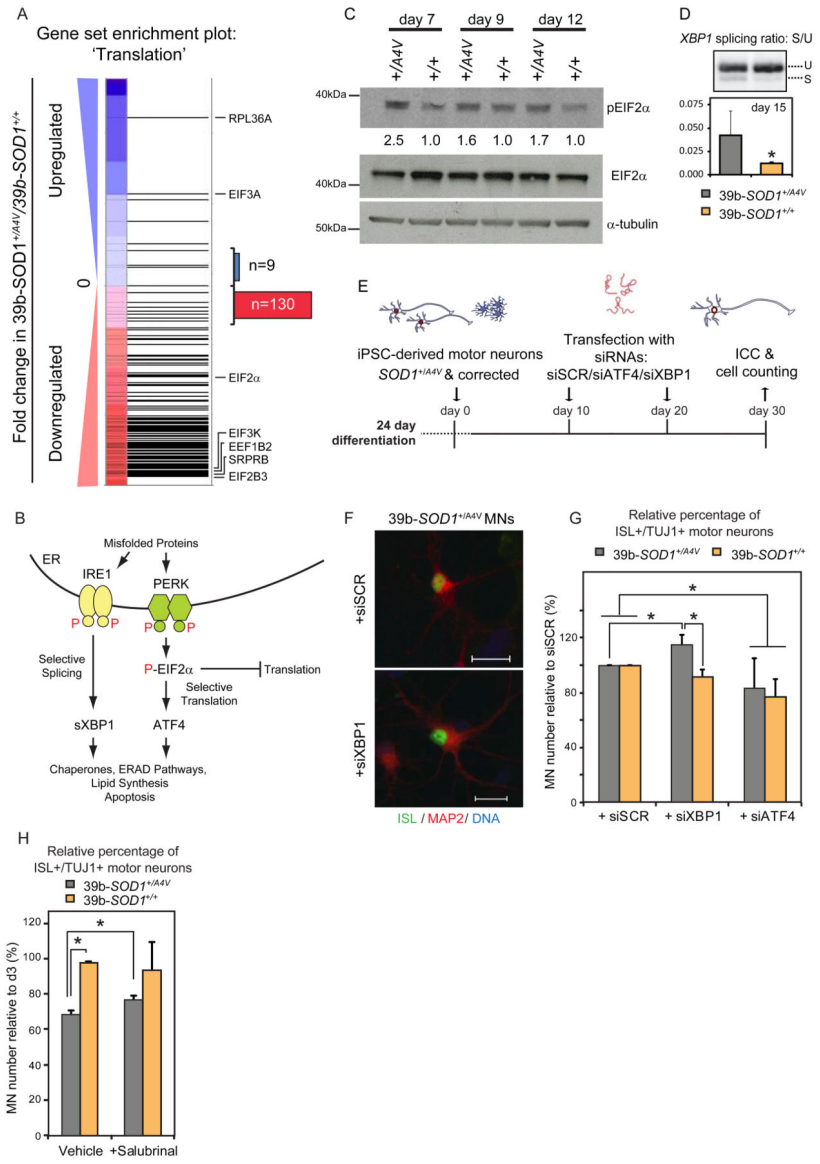


**Figure 5. *SOD1*$^{+/A4V}$ Motor Neurons Exhibit Signatures of an Unfolded Protein Response and are Selectively Vulnerable to ER Stress Induction**

**(A)** Gene set enrichment analysis of transcriptional changes in *SOD1*$^{+/A4V}$ MNs shows strong downregulation (normalized enrichment score: -3.31) for genes involved in translational capacity. Horizontal black bars represent individual genes with representative examples indicated. Blue or red represents genes which were up or downregulated respectively in *SOD1*$^{+/A4V}$ relative to isogenic control MNs. Out of 139 genes detected that are annotated as involved in regulation of translation, 130 were downregulated, consistent with activation of the UPR pathway. (**B**) Diagram illustrating the canonical unfolded protein response. (**C**) WB analysis demonstrates increased levels of phosphorylated EIF2α, a marker for activation of the UPR pathway, in *SOD1*$^{+/A4V}$ *MN* cultures. Percentage relative to control samples for each time point is shown. (**D**) *SOD1*$^{+/A4V}$ MNs exhibit increased levels of *XBP1* splicing, a marker of ER stress. RNA was isolated from purified *Hb9*: :RFP MNs after 15 days in culture (n=3, +/-SEM, P<0.05). U: unspliced, S: spliced. (**E**)

Experimental strategy used to assess the contribution of XBP1 and ATF4 in the survival of *SOD1*$^{+/A4V}$ MNs. (**F**) Representative images of untreated and treated MN cultures are shown. (**G**) *SOD1*$^{+/A4V}$ MN numbers selectively increase after *XBP1* knockdown, while *ATF4* knockdown significantly decreases numbers in both control and *SOD1+/A4V* cases (n=3, m>9800 and m>8500, P<0.05), +/-SEM, P<0.05). (**H**) Salubrinal has a modest but positive effect on survival of *SOD 1*$^{+/A4V}$ *MNs* (n=2, m>10000, +/-SEM, P<0.05).

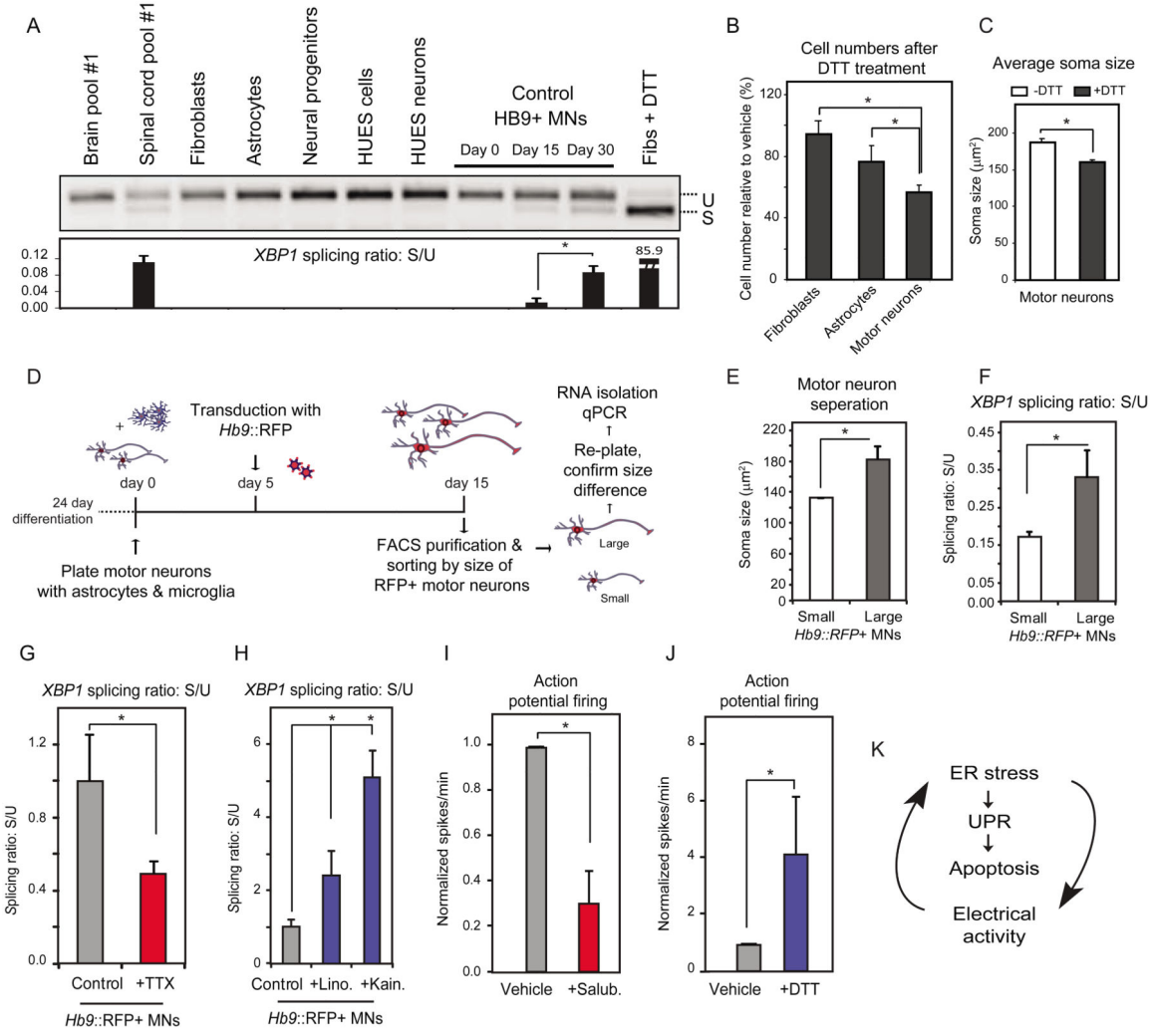


**Figure 6. Human Motor Neurons Exhibit Increased Levels of Basal ER Stress That is Dependent on Their Physiological Activity**

**(A)** Purified *Hb9*::GFP control MNs show higher levels of spliced *XBP1* relative to other human cell types. Human spinal cord RNA also shows higher levels relative to brain RNA. U: unspliced, S: spliced. (**B**) Control MNs are more vulnerable to acute ER stress induction (DTT, 2mM) relative to fibroblasts or astrocytes, while (**C**) DTT treatment leads to a reduction in MN soma size (n=2, +/-SD, P<0.05). (**D**) Experimental strategy used to isolate MNs based on cell size. Control MN cultures were infected with the *Hb9*::RFP virus on day 5. On day 15, RFP+ MNs were FACS-purified and sorted by size to separate small and large cells. (**E**) A subset of cells were re-plated to confirm soma size by measuring MAP2+ cell bodies (**F**). Basal levels of *XBP1* splicing were assessed in RNA isolated from the remaining purified MNs showing that larger MNs had higher spliced *XBP1* than smaller ones (n=3, +/-SEM, P<0.05). Treatment of MN cultures with (**G**) TTX reduces while (**H**) linopiridine and kainate increase *XBP1* splicing respectively. Treatment with (**I**) salubrinal reduces, while (**J**) DTT increases action potential firing (n=3, +/-SEM, P<0.05). **(K)** ER stress, the UPR and electrical activity of MNs are connected.

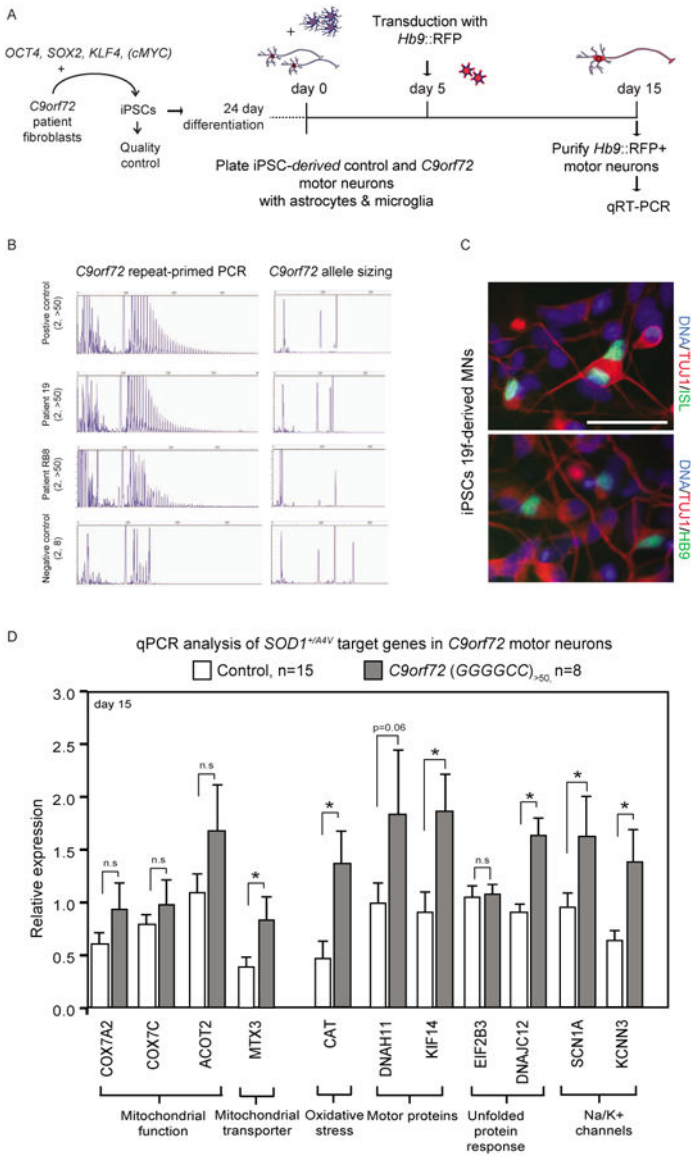


**Figure 7. Transcriptional Changes Detected in *SOD1*$^{+/A4V}$ Motor Neurons are Partially Conserved in Motor Neurons With *C9orf72* Expansions**

**(A)** Experimental outline: ALS patient fibroblasts harboring *C9orf72* repeat expansions were reprogrammed to generate iPSCs, which were differentiated into MNs and plated in co-culture with glial cells. On day 5 cultures were infected with an *Hb9*: :RFP lentivirus and on day 15, RFP-labeled MNs were FACS-purified for RNA isolation. (**B**) Genotyping of samples by repeat-primed PCR and allele sizing for *C9orf72*.Patient samples RB8 and 19 exhibited more than 50 *GGGGCC* repeats. (**C**) Representative images of MN cultures differentiated from *C9orf72* ALS patients (scale bar=50μm). (**D**) A subset of transcripts found to be differentially expressed in *SOD1*$^{+/A4V}$ MNs also exhibited significant transcriptional changes in MNs derived from *C9orf72* (n=2 lines, n=8 replicates, +/-SEM, P<0.05) compared to a large number of control samples (n=6 lines, n=15 replicates, +/-SEM, P<0.05).